A heating process of Kuchi-erabu-jima volcano, Japan, as inferred from geomagnetic field variations and electrical structure

Wataru Kanda[a,*], Mitsuru Utsugi[b], Yoshikazu Tanaka[b], Takeshi Hashimoto[c], Ikuko Fujii[d], Toshiaki Hasenaka[e], Nobuaki Shigeno[f]

[a] *Sakurajima Volcano Research Center, Disaster Prevention Research Institute, Kyoto University, Sakurajima-Yokoyama, Kagoshima 891-1419, Japan*
[b] *Aso Volcanological Laboratory, Graduate School of Science, Kyoto University, Minami-Aso, Kumamoto 869-1404, Japan*
[c] *Institute of Seismology and Volcanology, Graduate School of Science, Hokkaido University, N10W8 Kita-ku, Sapporo 060-0810, Japan*
[d] *Kakioka Magnetic Observatory, Japan Meteorological Agency, Kakioka, Ishioka 315-0015, Japan*
[e] *Department of Earth Sciences, Faculty of Science, Kumamoto University, Kurokami, Kumamoto 860-8555, Japan*
[f] *Seismological and Volcanological Department, Japan Meteorological Agency, Otemachi, Chiyoda-ku, Tokyo 100-8122, Japan*

Abstract

Since August 2000, we have recorded the total intensity of the geomagnetic field at the summit area of Kuchi-erabu-jima volcano, where phreatic eruptions have repeatedly occurred. A time series analysis has shown that the variations in the geomagnetic field since 2001 have a strong relationship to an increase in volcanic activity. These variations indicate thermal demagnetization of the subsurface around the presently active crater. The demagnetization source for the early variations, until summer 2002, was estimated at about 200 m below sea level. For the variations since 2003, the source was modeled on the basis of the expansion of a uniformly magnetized ellipsoid. The modeling result showed that the source is located at 300 m above sea level beneath the crater. We carried out an audio-frequency magnetotelluric survey with the aim of obtaining a relation between the demagnetization source and the shallow structure of the volcano. A two-dimensional inversion applied to the data detected two good conductors, a shallow thin one which is restricted to a region around the summit area, while the other extends over the edifice at depths between 200 and 800 m. These conductors are regarded as clay-rich layers with low permeability, which were assumed to be generated through hydrothermal alteration. The demagnetization source for the early variations was possibly located at the lower part of the deep conductor and the source after 2003 lies between the two conductors, where groundwater is considered to be abundant. Based on these results, as well as on seismological, geodetic, and geochemical information, we propose a heating process of the Kuchi-erabu-jima volcano. In the initial stage, high-temperature volcanic gases supplied from the deep-seated magma remained temporarily at the level around the lower part of the less permeable deep conductor since the ascent path had not yet been established. Then, when the pathway developed as a result of repeated earthquakes, it became possible for a massive flux of volcanic gases to ascend through the conductor. The high- temperature gases reached the aquifer located above the conductor and the heat was efficiently transported to the surrounding rocks through the groundwater. As a consequence, an abrupt increase of the gas flux and diffusion of the heat through the aquifer occurred and the high-temperature zone expanded. Since the high-temperature zone is located beneath another conductor, which acts as caprock, we assume that the energy of the phreatic explosion is accumulated there.

Key words: geomagnetic field, thermal demagnetization, electrical resistivity, phreatic explosion, volcanic fluid

1. Introduction

The proper evaluation of volcanic activity is an essential problem related to the forecasting of eruptions and the mitigation of volcanic hazards. It can be relatively simple for volcanoes where magmatic eruptions are expected based on historical experience since anomalous phenomena such as swarms of volcano-tectonic earthquakes or notable inflation of the ground are observed in the process of ascent of magma and are identified as precursors of eruptions (e.g. Ishihara, 1990; Voight et al., 1999; Nakada et al., 1999). However, conventional seismological or geodetic monitoring is generally insufficient in the case of volcanoes characterized by phreatic eruptions since the energy for the impending eruption is not large and can accumulate even without magma movement (Barberi et al., 1992). It is necessary to know the state of the hydrothermal system developed within such volcanoes in order to obtain a more detailed understanding of the area where phreatic eruptions are expected.

Continuous observation of the total geomagnetic intensity is often employed for evaluation of volcanic activity due to its capability for revealing the condition of energy accumulation within active volcanoes. This method utilizes the characteristics of igneous rocks: the magnetization increases or decreases due to changes in the physical conditions, such as stress or temperature. Numerous attempts have been made to monitor the state of the crustal stress or the temperature within the volcano through the observation of geomagnetic fields at the surface, and volcanomagnetic variations related to the anomalous volcanic activities have been reported for a large number of volcanoes (e.g. Mount St. Helens by Johnston et al., 1981; Izu-Oshima volcano by Yukutake et al., 1990; Aso volcano by Tanaka, 1993; Merapi volcano by Zlotnicki and Bof, 1998; Etna volcano by Del Negro et al., 2004; White Island volcano by Hurst et al., 2004).

The reported volcanomagnetic variations occur on different timescales ranging between one day and a few years, and have different amplitudes ranging between several to over 100 nT. The timescale fluctuations depend on the speed of change of the physical conditions of the volcano and on the mechanism of generation of anomalous magnetic fields. The timescale is generally longer than that of other mechanisms if the mechanism is thermal remagnetization or demagnetization of igneous rocks. Furthermore, the amplitude fluctuations strongly depend on the separation between the observation site and the source of the variations, although they also depend on the rock type. In general, large amplitudes are observed at volcanoes composed of basaltic rocks compared to volcanoes composed of andesitic or dacitic rocks. Tanaka (1993) reported that a large amplitude of the variation ($\sim$ 30 nT) was observed at Aso volcano by installing magnetic stations in the vicinity of the presently active crater.

Kuchi-erabu-jima is a volcanic island located about 80 km south of Kyushu Island, in southwest Japan (Fig. 1(a)). After the oldest historical record of an eruption there, dating from 1841, phreatic or phreatomagmatic explosions have occurred repeatedly at intervals of several years to a few tens of years. During the 1933-1934 eruption activity, a village located at the eastern foot of the volcano suffered serious damage from the volcanic bombs (Tanakadate, 1938). The latest explosion occurred in 1980 and volcanic activity ceased for more than 20 years after that.

In recent years, however, an increase in the seismic activity was observed beneath the summit area, in 1996 and 1999 (Yamamoto et al., 1997; Iguchi et al., 2001). It was assumed that these events marked the preparation process for the impending phreatic explosion. Temporary seismic observations were performed before past eruptions, although no clear precursory signals were reported (Iguchi et al., 2007). Since the volcano gave rise to repeated phreatic explosions, we planned a continuous geomagnetic observation aimed

*Corresponding author. Tel.: +81 99 293 2058; fax: +81 99 293 4024.
Email addresses: kanda@svo.dpri.kyoto-u.ac.jp (Wataru Kanda)

at monitoring the underground thermal state. It was hypothesized that if the temperature of the area increased sufficiently to reduce the magnetization of the volcanic rocks, it might be possible to observe the changes in the total geomagnetic intensity at the surface.

Furthermore, the area was studied on the basis of the subsurface structure. We aimed to reveal the electrical resistivity around the expected preparation area as well as to provide certain constraints on the involvement of the volcanic fluids for the accumulation of thermal energy.

Kuchi-erabu-jima volcano lies in the central part of the island and consists of a stratovolcano complex whose massif is mainly composed of three volcanic edifices: Shin-dake, Furu-dake, and No-ike (Fig. 1(b)). Shin-dake and Furu-dake have presently active craters on their summit areas. Most of the igneous rocks in the island are composed of pyroxene andesite with SiO_2 content of 54~62 % (Matsumoto, 1960; Geshi and Kobayashi, 2006). All volcanic events for at least the past 200 years originated from the Shin-dake crater or from its surroundings. The diameter of Shin-dake is about 250 m and the depth to the bottom is about 100 m. A NNE-SSW trending fissure with a length of about 700 m is observed at the eastern side of the crater. There are fumaroles with an outlet temperature of about 100 °C around the western to southern rim of this crater. Although there is no eruption record for Furu-dake, a magmatic eruption was inferred several hundred years ago (Geshi and Kobayashi, 2006). The Furu-dake crater also has intensive fumaroles with sublimates of sulfur around it. No-ike is the oldest of three volcanoes and is inactive, with no geothermal manifestation.

2. Geomagnetic field data

Three Overhauser magnetometers (GSM-19, GEM systems Inc., Toronto) were installed at the summit area of Kuchi-erabu-jima volcano in August 2000 and measurements with a sampling interval of 5 minutes have been conducted since then (A1, B1, and C1 in Fig. 1(c)). GSM-19 has a resolution of 0.01 nT with 0.2 nT absolute accuracy. Since the measured data are stored into internal memory, it is necessary to retrieve them on site once every several months. Only the hourly averaged values are sent via satellite telecommunication service (Orbcomm system) for monitoring purposes (Kanda et al., 2001). The distribution of the magnetometers was designed to effectively detect thermo-magnetic effects based on the assumption that the demagnetized area is located directly beneath the Shin-dake crater around the hypocenters of the volcanic earthquakes (Yamamoto et al., 1997). In addition, two proton-precession magnetometers (PM-215, Tierra Tecnica, Tokyo) have been obtaining data at intervals of 1 minute since May 2002 (P2 and P3 in Fig. 1(c)). These detectors were installed to obtain spatially detailed information regarding the volcanomagnetic variations originating from Shin-dake. PM-215 had the same resolution as the other magnetometer and an accuracy of 0.1 nT. The data were stored on a flash memory card and was also telemetered through a cellular phone or a radio communication system. All magnetometers and telemeters were powered by 12 V DC batteries continuously charged by solar panels.

Figure 2 shows the daily means of the total intensity observed at five sites at Kuchi-erabu-jima volcano and at the Kanoya Magnetic Observatory (KNY) of the Japan Meteorological Agency (JMA) between August 2000 and January 2008. Since the observation was automatically operated on the remote island, there are gaps in the data due to power issues or machine failure at various times. In particular, as Kuchi-erabu-jima is located on the path of typhoons in the summer season, the magnetometer at A1 suffered serious damages several times. As a result, discontinuity occurred for the data acquired at A1 between December 2002 and June 2003 due to this reason, although the continuity of the measurement was retained at other sites. The long-term trends at most sites, as well as those of KNY, appear to decrease, which indicates that regional-scale secular variations tend to decrease.

Figure 3 shows the simple differences of the total intensities at five sites at Kuchi-erabu-jima from those at KNY. It is clear that the tendencies in variations observed at sites located north of the Shin-dake crater are different from those observed south of the crater. The total intensities have increasing tendencies as compared to KNY at sites A1 and P2, which are located north of the crater, while it decreases at sites B1, C1, and P3, which are located south of the crater. In this regard, the variations shown in the three lower panels are particularly prominent. The total deviation after 2001 reached about 70 nT at C1. This variation pattern is expected when demagnetization occurs beneath and around the Shin-dake crater. The slow variations suggest that the cause of the demagnetization is a change in temperature within the volcano.

3. Volcanomagnetic variations and their origin

3.1. Estimation of volcanomagnetic variations

The simple difference technique implicitly assumes that both the secular variations and the magnetic fields of external origin at Kuchi-erabu-jima are identical to those at KNY. Therefore, estimates of the variations may contain uncertainties. Volcanomagnetic variations are regarded as a component which varies slowly and locally due to the thermal processes dominating the inside parts of the volcano. We estimated the trend component for each site by using a time series analysis in which the magnetic field of external origin can be efficiently removed (Fujii and Kanda, 2008).

A time series model used for estimating the trend component decomposes a field $f(i)$ observed at time i into four components: trend $t(i)$, periodic component $s(i)$ with a period of J, externally correlated component $r(i)$, and observation noise $w(i)$.

$$f(i) = t(i) + s(i) + r(i) + w(i) \tag{1}$$

The constraints applying to each component are as follows.

$$t(i) - 2t(i-1) + t(i-2) = u(i) \tag{2}$$

$$\sum_{j=0}^{J-1} s(i-j) = v(i) \tag{3}$$

$$r(i) = \sum_{j=1}^{3} \sum_{k=-L}^{K} \left[A_j(k) x_j(i+k)\right] \tag{4}$$

where u(i) and v(i) are uncertainties which obey Gaussian distributions with a mean of 0 and a variance τ_t^2 and τ_s^2, respectively. Furthermore, $x_j(i)$ is a given time series of the j-th reference. We commonly use three components of the geomagnetic field observed at a reference station, and the data recorded at KNY were used in this study. K and L denote the maximum number of data points at the reference station in the past and the future, respectively. Observation noise $w(i)$ is also assumed as a Gaussian with a mean of 0 and a variance τ_o^2. The above equations were represented as a state-space model and were solved by applying a Kalman filter algorithm (Fujii and Kanda, 2008). We fixed τ_t^2 to 10^{-5} in order to obtain a smooth trend. Regarding J, $J = 12$ was used for the hourly data in order to account for oceanic and ionospheric tides, and other hyper-parameters controlling the four components were determined as follows: the maximum likelihood estimate was adopted in order to determine τ_s^2 and τ_o^2. The parameter τ_o^2 represents the variance of the noise component $w(i)$, which is a measure of misfit between the observed and the estimated time series. The values for K and L were selected in such a way as to minimize AIC (Akaike, 1973).

We estimated each component of Eq. (1) for the hourly means of the observed 7.5-year-long data set for the period between August 2000 and January 2008. The estimated trend components for the five sites are shown in Fig. 4 and the optimal parameters for obtaining these trends are listed in Table 1. As the simple difference data suggests (Fig. 3), the characteristic trends of variations most likely related to the thermal demagnetization beneath and around the Shin-dake crater are obtained. Starting from around May 2001, the site A1, located at the northern side of the crater, shows a tendency of increase, while the trends at C1 and B1, located on the southern side of the crater, tend to decrease. The same tendency can be observed for the variations at the two other stations at which the observation started in May 2002, where the site P2, located north of the crater, shows a tendency of increase, while the site P3, located south, shows a tendency of decrease.

The variations at C1 and P3 appear to cease by early 2006, after which a tendency of slight increase is observed until August 2006. However, the trends at A1 and B1 also show similar trends, and the variations after 2006 are comparable for all sites. It is unclear whether these variations are caused by the remagnetization of rocks. The volcanomagnetic variations resume in August 2006, and rapid changes are seen at all sites except B1. These changes continue until the latter half of 2007 with slowing variation rates. The total decrease of the field is about 62 nT at C1 and 43 nT at P3 by January 2008.

As an example, in Fig. 5 we show the misfit between the observed and the estimated time series ($w(i)$ in Eq. (1)) for site C1. The residual in most periods is lower than ± 3 nT for the hourly values and lower than ± 1 nT for the nighttime means. Variations shown in Fig. 4 are considerably larger than this error level. Larger residuals are seen when the local noise was contaminated or when intensive magnetic storms occurred, although these are temporary phenomena. The trend itself is not affected by these disturbances. Larger residuals are also obtained for the first several hours of the data set, which is caused by the use of inaccurate initial values provided to the Kalman filter algorithm (Fujii and Kanda, 2008).

3.2. Model of demagnetization source

We modeled the magnetic source causing the volcanomagnetic variations presented in the previous section (Fig. 4) under the assumption that these variations are entirely due to the demagnetization of rocks. The total intensity changes over a given period of time were modeled by estimating an equivalent magnetic dipole. As shown in Fig. 4, four periods were selected (prd.1∼4) in consideration of the data gaps and the change in variation rates, where the position and the moment of the magnetic dipole, which were estimated in each period by a grid search, were taken as unknowns. The grids of the position were set with intervals of 25 m around the Shin-dake crater, and those of the magnetic moment was set with every an exponent of 1.25 Tm^3, respectively. The direction of magnetization was assumed to be parallel to the current geomagnetic field at Kuchi-erabu-jima (inclination of 43 ° and declination of -6 °).

Since there is a limited number of observation sites, a set of optimum parameters was estimated to measure their diversity by applying a bootstrap method (e.g. Efron and Tibshirani, 1993). The brief description of the method we used is as follows. At first, model parameters that minimize the sum of the squared residuals at the observation sites are searched for by the grid search. Then, a resampled set of the residuals that is randomly drawn from the set of the residuals allowing duplication is added to the data set in order to create a synthetic data set (a bootstrap sample). The optimum parameters against the bootstrap sample are searched for again by the grid search. These procedures were repeated for 200 bootstrap samples.

For prd.1, only the data of three observation sites are available, we imposed additional constraints on the expected changes at P2 and P3. As seen in Fig. 4, the magnitude of the geomagnetic changes at P2 and P3 does not exceed that at C1 throughout the record, and as a result we adopted the model which expected that changes at P2 and P3 did not exceed 1.25 times the magnitude of the changes at C1. The mean and the standard deviation of each parameter estimated from 200 bootstrap samples in each period are shown in Table 2 and Fig. 6.

The dipole source for prd.1 is located beneath the SSE rim of the Shin-dake crater at about 200 m below sea level (bsl). On the other hand, the source locations are estimated at almost the same position of about 300 m above sea level (asl) beneath the Shin-dake crater from prd.2 to prd.4, although the magnitude of the magnetic moment is likely to increase gradually.

It should be noted that the source location estimated in prd.1 has a larger uncertainty than those in the other periods because of a small number of the available observations and a data gap at B1. The estimated depth of the source in prd.1 depends on the magnetic changes observed at B1 that is a distant site from the crater. The B1 data has a gap between August and October 2001 (Fig. 4), which was caused by a mistuning of the magnetometer. Most of the magnetic change in prd.1 appears to have occurred during the gap. Since we confirmed that the sensor position did not change before and after the gap, we assumed that the obtained magnetic change at B1 is volcanic. In addition, the variation at each site may start at different timings during prd.1, which could imply that multiple sources contributed to the observed variations. For simplicity, we assume in Table 2 that the changes are caused by a single dipole source.

If the dipole source is located at a sufficient distance, the magnetic moment is equivalent to the product of the volume of a uniformly demagnetized sphere multiplied by the magnetization change (ΔJ). On the other hand, in case of a short distance between the source and the observation site, the observed magnetic changes can not be explained by using the spherical demagnetization source since the shape of the source affects the resulting magnetic field. The dipole sources after prd.2 were inferred at the shallow place inside the observation network (Fig. 6), where the effect of the shape can be estimated from the data. If we assume a relatively simple shape, we can estimate the demagnetized volume and can also assume certain constraints regarding the magnetization changes.

Next, we attempted to fit the total intensity changes from prd.2 to prd.4 observed at each site to the magnetic anomaly produced by a uniformly demagnetized triaxial ellipsoid (Clark et al., 1986; Sasai, 2006). Modeling by a triaxial ellipsoid was first introduced to interpret the volcanomagnetic changes observed at Taal volcano, the Philippines, by Zlotnicki et al. (2009). In this modeling, certain assumptions were additionally imposed in order to reduce the number of unknown parameters. The estimation results for the magnetic dipole sources imply that the demagnetized zone expanded at the same position after prd.2. The center of the ellipsoid was assumed to be the same throughout the three periods, and the axis lengths at the later period are larger than those in prd.2. To avoid complexity, each axial direction of the ellipsoid was set to the direction as a coordinate axis, and the parameters to be estimated were set as the coordinates of the center of the ellipsoid, its half-axis lengths, and the magnetization change during the period. The optimum parameters were estimated by a grid search, and are shown in Table 3. The grids of the position and the axis lengths were set with an interval of 20 m, and the magnetization change was 0.1 A/m in this calculation.

In Fig. 6, the estimated demagnetized zones between prd.2 and prd.4 are shown with ellipses. Ellipsoidal demagnetized zones have an E-W trending shape whose center is located at 300 m asl beneath the Shin-dake crater. In prd.2, the lengths of the half-axis are 40 m in N-S direction, 80 m in E-W direction, and 140 m in vertical direction, which expand horizontally during prd.3 and prd.4 to 100 m along the N-S axis and 120 m along the E-W axis, while the length along the vertical axis remains the same. The expected magnetic changes at the ends of prd.2 and prd.4 are shown in Fig. 7 together with the volcanomagnetic variations after prd.2.

These results indicate that the demagnetization at the shallow part beneath the crater occurred in early 2003 when the magnetic variations at sites C1 and P2 changed their variation rates prior to prd.2 (Fig. 4) and fumaroles appeared at the bottom of the crater. Although we do not have the measurement data of the ground temperature, airborne thermal infrared images were repeatedly obtained (Iguchi, 2007). In the first measurement carried out in February 2001, geothermal anomaly was not recognized in the crater bottom (temperature below 20 °C). However, by the second measurement in March 2003, obvious geothermal anomaly inside the crater with the highest temperature of 38 °C was observed. If the demagnetization is caused by a sudden surge of heat, the expansion of the demagnetized area can be interpreted as the expansion of the high-temperature area beneath the area around the southern part of the Shin-dake crater, which is consistent with the observed surface phenomena, such as the increase in fumarolic activity or the expansion of the thermal anomaly around the crater.

3.3. Rock magnetization and temperature dependence

In the previous section, uniformly demagnetized ellipsoids with intensities of 1.8 and 1.9 A/m were used as a model causing the observed volcanomagnetic variations between prd.2 and prd.4. Since Kuchi-erabu-jima is an andesitic volcano, the magnetization intensity of volcanic rocks is considered to be low. Miki et al. (2002) measured the natural remanent magnetization (NRM) of ten rocks sampled from four lava flows and found that the mean intensities are between 1.4 and 13 A/m. Among these, only two rocks sampled from the lower lava flow showed 1.4-1.6 A/m, while others showed values larger than 6 A/m, indicating that the lava of Kuchi-erabu-jima is generally characterized by large NRM. However, the observed magnetic variations were not always caused by cold lava which has been magnetized at the surface of the ground. Utsugi et al. (2002) estimated the distribution of apparent magnetization from an aeromagnetic survey over Kuchi-erabu-jima and showed that the magnetizations were low (less than 2 A/m) around the summit area and high (about 5 A/m) at the flanks of the volcano.

To examine the validity of the estimated changes in magnetization intensity, we measured the NRM and the magnetic susceptibility for eleven rocks ejected in recent eruptions. The rocks were collected at the summit area of Kuchi-erabu-jima volcano. All measurements were performed inside a magnetically shielded room where the remaining magnetic field was less than 50 nT (Miki, 1995). The averages for 3 to 7 samples from each rock are summarized in Table 4, where the NRM is between 0.5 and 18 A/m, with a relative errors of less than 2%. Three of 11 rocks show large NRM values of more than 5 A/m, while the NRM for the others is less than 2 A/m. A number of rocks with weak NRM had partly hydrothermally altered components.

The induced magnetizations were calculated from the measured susceptibilities assuming the present geomagnetic field intensity on Kuchi-erabu-jima as 46,000 nT. In a group of rocks with weak NRM, a number of rocks had comparable induced magnetization (Q = 0.4−1.3 in Table 4), while members of the other group had relatively small induced magnetization (Q = 4.3−12).

Figure 8 shows the remaining magnetization of eleven rocks as a result of a stepwise thermal demagnetization. The magnetization is normalized by the initial value for each rock measured at room temperature before the experiment. The magnetization of four rocks denoted with squares decreases by about 20% at 120 °C and more than 80% at 400 °C, indicating that titano-magnetite is the dominant component. The NRM values of these rocks are small (0.6-1.2 A/m, shown in Table 2), which is insufficient for a magnetization change of about 2 A/m even if they are completely demagnetized. Three rocks denoted with circles have large NRM values of 5-18 A/m. Since the magnetization is almost completely lost at 590 °C, it is concluded that magnetite is dominant in these rocks and can be regarded as the predominant component for the estimated change in magnetization.

It appears that the characteristics of the remaining four rocks (triangles and stars) are between those of the two rocks discussed above according to the content of the titanium component. However, it is clear that the features of the two rocks denoted with stars, whose remanent magnetization is still more than 10% at

590 °C, are different. It is hypothesized that these two rocks contain other components, such as maghemite or hematite, which have suffered a high-temperature oxidation at the time of eruption.

If magnetite-rich rocks are heated to 500 ° C beneath the Shin-dake crater, a magnetization change of about 2 A/m would be easily obtained. In this case, rocks containing titano-magnetite lose most of their magnetization.

4. Electrical resistivity structure

We carried out an audio-frequency magneto-telluric (AMT) survey in November 2004. The objective of the survey was to obtain a relationship between the demagnetized area and the resistivity structure. As shown in Fig. 9, AMT data were collected at intervals of about 500 m. The data over the frequency range between 1 and 10,000 Hz were recorded for 11 hours at night by using three MTU-5A systems (Phoenix Geophysics Ltd.). A special site for remote reference was not installed, although multiple sites were used at the same time during the night, which allowed the researchers to reference each other.

Since the impedance skews were less than 0.2 at all sites for all usable data, we assumed that the subsurface structure of this region is two-dimensional (Bahr, 1991) and estimated the strike direction. The inset of Fig. 9 shows the distribution of the strike estimates for frequency-dependent and site-dependent decompositions (Groom and Bailey, 1989). Most of the data was between N5°E-S5°W and N20°E-S20°W or between N85°W-S85°E and N70°W-S70°E due to the ambiguity of 90 degrees. The real induction arrows (Parkinson, 1962) at 97 Hz are also shown in Fig. 9. The arrows tend to point towards the summit area, suggesting that the presence of resistivity contrasts along the profile, and a conductive region is expected around the summit area. This feature is also seen at lower frequencies. Considering that the volcano has the summit craters aligned along the N-S direction, N13°E was assumed as the strike direction in this study.

A 2-D inversion (Ogawa and Uchida, 1996) was applied to the data set corresponding to the direction which is nearly perpendicular to the estimated strike direction (Fig. 9). Static shift was not corrected; instead, it was included as an inversion parameter. We used only the TM-mode apparent resistivity and phase data for the inversion. Since Kuchi-erabu-jima is an island surrounded by the sea, we also included the bathymetry in the model and fixed the resistivity of sea water to 0.33 Ωm. The error floors for both the apparent resistivity and the phase were set to 10%. The final resistivity model with the root mean square (RMS) misfit of 0.95 is shown in Fig. 10, while the pseudo-sections of the observed data and the inverted results are shown in Fig. 11. Most of the features of the observed data can be explained by the inferred model. The inversion with no static shift was tested and the resultant resistivity structure showed a remarkable similarity to Fig. 10.

The inferred model has the following characteristics. Since borehole data are unavailable for Kuchi-erabu-jima, we interpret the resistivity model on the basis of geologic information (Geshi and Kobayashi, 2006, 2007). First, high resistivities greater than 1,000 Ωm and several hundreds Ωm are recognized near the surface of the WNW flank (R1 in Fig. 10) and the ESE flank (R2). These resistivities correspond to the permeable lava of Shin-dake and Furu-dake, respectively. The Shin-dake lava is distributed only on the western to northwestern side of the edifice and is composed of at least three flow units. Paleomagnetic studies have estimated the eruption date for these lava flows at about 900-1,100 years ago (Miki et al., 2002; Matsumoto et al., 2007), and the age of Furu-dake lava has been estimated in the range between 11,000 and 3,000 years before present by using tephrochronology (Geshi and Kobayashi, 2006). The difference in resistivity values between the WNW and the ESE flanks is attributable to the degree of weathering or alteration.

Two conductive regions can be recognized. One is a conductive layer near the surface beneath the summit area which extends to the flank of Furu-dake (HCa). The other is a thick layer over the edifice at depths between 200 and 800 m (HCb). These conductive regions are likely to be related to the presence of conductive clay minerals, such as smectite, resulting from the hydrothermal alteration. Such altered materials have been detected in the volcanic ash of a phreatic eruption in 1980 (DPRI et al., 1981; Tomita et al., 1994) and even in the large volcanic bombs ejected by the phreatomagmatic eruption in 1966 (Aramaki, 1969). HCa is formed due to the elevated temperature beneath the area around the active craters. Highly conductive layers regarded as the region containing conductive clay species have been found beneath a large number of other andesitic volcanoes (e.g. Nurhasan et al., 2006; Kanda et al., 2008).

Next, the origin of HCb is considered. Geshi and Kobayashi (2006) estimated the evolution process of Shin-dake and Furu-dake as follows. Older Furu-dake started erupting at around its present center on the southern flank of No-ike about 13,000 years ago. A major sector collapse opened to the south occurred between 11,000 and 5,000 years ago at the summit area, after which Younger Furu-dake emerged to fill the collapsed edifice. After Furu-dake collapsed again to the northwest between 3,000 and 1,000 years ago, Shin-dake evolved from the exposed flank of Older Furu-dake. The remained rims of the slope failures are shown in Fig. 1 with gray lines. This geologic evidence suggests that this highly conductive layer (HCb) corresponds to the past edifices of Older Furu-dake and No-ike (Fig. 10), and forms structural boundaries between Shin-dake / Younger Furu-dake and Older Furu-dake.

Regarding the reason why the edifice of Older Furu-dake is conductive, we consider two possibilities. One is that the upper part of HCb in Fig. 10 is composed of the brecciated and altered clay-rich rocks produced in the two major sector collapses. A similar case was reported for the La Fournaise volcano, where a highly conductive basement was found at a depth of a few hundred meters, and has been interpreted as a layer of clay-rich brecciated rocks resulting from the landslides (Courteaud et al., 1997; Lénat et al., 2000). Another possibility is that the hydrothermally altered layer had already developed within Older Furu-dake before the collapses since hydrothermal processes often play an important role in volcanic sector collapses (Lopez and Williams, 1993).

In Kuchi-erabu-jima, groundwater is abundant within the massif. As seepage of groundwater can be found at different places at the foot of the volcano, it is assumed that an aquifer is formed around the upper boundary of the conductive layer (HCb) since such a hydrothermally altered clay-rich layer is generally impermeable and meteoric water is accumulated through permeable volcanoclastics near the center or through permeable lava on the flanks (R1, R2). In this case, it is assumed that the moderately conductive layer of less than several tens Ωm immediately above the HCb layer acts as a saturated water table. Hirabayashi et al. (2002) pointed out that hot spring water sampled near the coast at the northern foot of the volcano is affected by hydrothermal fluids of magmatic origin since the composition of the water showed unusually high content of SO_4^{2-}. The inferred demagnetized zone between prd.2 and prd.4 is located at the upper boundary of HCb, and the dipole source for prd.1 is around the bottom of HCb (Fig. 6). Hydrothermal fluids are likely to be related to the mechanism of the thermal demagnetization process.

A somewhat resistive layer of less than 100 Ωm is seen below HCb. We tested the sensitivity of the central part of this layer by changing the resistivity value to 1 Ωm. As a result, most of the observed data were unaffected by this modification, and the consequent RMS misfit of 0.98 was slightly larger than that of the final model (Fig. 10). Therefore, we regard this resistive layer as less sensitive and do not discuss it in this study.

5. Discussion

Our results indicate that the demagnetization center after 2003 is located above the widely spread conductor (HCb in Fig. 10). We discuss the source location and the mechanism of demagnetization with seismological, geodetic, and geochemical data.

5.1. Seismological data

Seismic activity has been monitored since 1991, when a seismometer was installed at the western flank of the volcano by the Disaster Prevention Research Institute (DPRI) of Kyoto University (DPRI, 1992). In recent years, high seismic activity at the summit area was observed in 1996 and 1999. Figure 12 shows the monthly number of volcanic earthquakes and the observed geomagnetic field variations at site C1 since August 2000. After the swarm activity in 1999, seismicity at Kuchi-erabu-jima has generally remained high. An episode of sudden increase of the number of earthquakes is repeatedly observed almost every year. Most of these earthquakes are high-frequency (HF) events with dominant frequencies higher than 5 Hz, although low-frequency (LF) events (1-4 Hz) or monochromatic (MC) events (1-30 Hz) also occur (Iguchi et al., 2001). The typical source mechanism of HF events is the normal-fault type with a WNW-ESE extension axis (Iguchi et al., 2001; Triastuty et al., 2009).

A volcanomagnetic field variation starts around May 2001, when a rapid increase in the number of earthquakes is observed. In addition, changes in the variation rate are observed in early 2003, at the end of 2004, and in the middle of 2006. Correspondingly, the temporal increase in seismic activity occurs nearly at the same time.

The hypocenters of the HF events were located beneath the area around the Shin-dake crater at around sea level as inferred from a temporary observation in 1996 (Yamamoto et al., 1997), and shallower hypocenters (0-400 m asl) were inferred in 2001 (Iguchi et al., 2001). The foci of the LF events were also determined in the 1996 campaign at nearly the same locations as those of the HF events. These hypocenters are located above the demagnetization center for prd.1 and in the HCb, suggesting that HF earthquakes do not occur in high-temperature areas.

Triastuty et al. (2009) located volcanic earthquakes occurred in 2006 by using the permanent seismic network around the Shin-dake crater established in 2002. They determined that the hypocenters of HF, LF, and MC events are located at depths shallower than 200 m asl, 400 m asl, and 300 m asl, respectively. The focal region of these earthquakes extends from the upper boundary of the highly conductive layer (HCb) to the bottom of the crater, penetrating the moderately conductive layer regarded as the aquifer as well as another highly conductive HCa layer. This distribution of the hypocenters corresponds to the upper margin of the ellipsoidal demagnetized zone, and, in particular, all LF events occur above this zone. This feature is similar to that of the hypocenters as obtained in 2001.

During the elevated seismic activity starting in August 2006, the number of earthquakes from different types reached their respective peaks at different times in the order of MC, LF, HF. Iguchi et al. (2007) interpreted this sequence as follows. The number of MC events increased in August 2006 at the initial phase of the upward migration of volcanic fluids, after which the LF activity increased in October due to a high fluid flux. Finally, a large number of HF events occurred in November as a result of brittle failure of the rocks around the inflated pressure zone caused by fluid migration as the pressure was gradually released by gas emission through fumaroles. The obtained volcanomagnetic variations during prd.4 indicate that abrupt demagnetization started in August 2006. This evidence can be explained if we assume that fluids with large heat capacity are present around the demagnetized area. This is consistent with our interpretation that the aquifer is formed around the upper boundary of the conductive layer (HCb) inferred from the AMT survey. The high-temperature volcanic gases supplied from the deeper parts reach the aquifer and heat is transported rapidly to the surrounding rocks through the fluids. Simultaneously, the fluids continue rising toward the crater, causing MC and LF.

5.2. Geodetic data

Global Positioning System (GPS) surveys have been repeatedly conducted since 1996 and have detected the radial pattern of horizontal displacements around the Shin-dake crater, which indicates inflation within the volcano (Iguchi et al., 2002). The inflation has been interpreted by using a point source model, and the position has been estimated at 100 m bsl 500 m east of the crater from the data sets obtained in 1995/96 and in 2000. We observed the elevated seismic activity in 1999, but the relation of this activity to the ground deformation is unclear because of the campaign observations. The depth of the inflation source almost coincides with that of the demagnetization source estimated during prd.1 (Table 2). If the two different sources are related each other, one possible interpretation is that the migrated volcanic gases reached the low permeable layer (HCb) and temporarily remained around the lower part of HCb, which caused the increase of pressure in that region.

The ground deformation beneath the Shin-dake crater has been monitored by using a continuous GPS network since April 2004 (Saito and Iguchi, 2006, 2007). The outstanding extension of the baselines between the summit and the flank stations indicating an inflation of the volcanic edifice was observed between January and May 2005 as well as between September 2006 and January 2007 in concordance with the high seismic activity (Fig. 12). The elevation of the inflation source was estimated at 250-300 m asl in 2005, assuming that the source was located beneath the center of the Shin-dake crater. The repeated surveys also detected a distinct inflation pattern from the data set obtained in February 2005, January 2006, and December 2006 / February 2007. The location of the inflation sources was estimated to be beneath the Shin-dake crater at 200 m asl during 2005 and 370 m asl during 2006 (Iguchi et al., 2007). These sources are located in the ellipsoidal demagnetization zone, which supports the view of our model that pressure in the aquifer increased due to the continuous supply of high-temperature volcanic gases.

The pressurized rocks can produce piezomagnetic variation (e.g. Sasai, 1991; Zlotnicki and Bof, 1998; Del Negro et al., 2004), although the piezomagnetic effect is generally small compared to the thermal effect. The expected variation pattern is opposite to the thermal demagnetization, although such variation (increase at sites located south of the source and decrease at sites located north) is not observed (Fig. 4).

5.3. Geochemical data

Next, geochemical studies of fumarolic gases should also be considered. Researchers at Tokyo Institute of Technology have repeatedly sampled and analyzed volcanic gases of the fumaroles located at the eastern (CR-E), southern (CR-S), and the western (CR-W) rims of the Shin-dake crater since 1992 (Hirabayashi et al., 2002, 2007). CR-E is located at the southern part of the fissure which erupted in 1980 and gradually declined in activity, making it impossible to obtain gas samples after 2004. Alternatively, the fumarolic activities of CR-S and CR-W have become dominant since 2003. It has been reported that SO_2 and H_2 were included in the fumarolic gases in high concentration, and CO have also been detected from both fumaroles. These components are characteristic of high-temperature gas of magmatic origin, and sporadic increases in concentration of these components have been observed since 2005. Another important result from the chemical component analysis is that hydrogen chloride (HCl) has not been detected (Hirabayashi et al., 2007). This implies that degassed HCl (as well as SO_2) is absorbed by groundwater as HCl is highly soluble in water and that the magma body is considered to be located further down below the aquifer.

The outlet temperature has remained unchanged at about 100 °C since April 2003, while the apparent equilibrium temperature (AET) estimated from the chemical composition of fumarolic gases at CR-S and CR-E has shown very high values of 450-550 °C. AET is the equilibrium temperature of the reaction of SO_2 / H_2S and is one of the indicators of the subsurface thermal state (Ohba et al., 1994). These AET values are consistent with our estimated temperature of the demagnetized rocks. Hirabayashi et al. (2007) explained that the large difference between the outlet temperature and AET was caused by the rapid cooling of volcanic gases by groundwater, which is widely spread within the volcano. The presence of groundwater is implied by the results of our AMT survey.

5.4. *Thermal demagnetization process*

Surface geothermal anomalies have been observed since February 2003 in concordance with high seismicity (Iguchi, 2007). Fumaroles appeared at the northern side of the bottom of the crater, where eruptions occurred in 1933 (Tanakadate, 1938). Intense fumarolic activity has been observed around the crater since February 2005 (Fig. 12). All available data indicate that the thermal state of shallow subsurface around the Shin-dake crater is characterized by extremely high temperatures.

A conceptual model of thermal demagnetization is shown in Fig. 13. As for the early source, we suggest the model as a possible mechanism because there are uncertain factors. High-temperature volcanic gases transport the heat from deep-seated magma. The heating process as inferred from this study is as follows.

1. It is reasonable to consider that the high seismic activity in 1996 and 1999 was induced by the ascent of volcanic gases within the less permeable layer (HCb) since the hypocenters of the earthquakes in 1996 were determined to be around sea level. The ascent path was rather narrow and had been maintained since the 1980 eruption due to the fact that fumarolic activity was intermittently observed.
2. In spring 2001, the high-temperature gases which were unable to pass through HCb were accumulated around the lower part of HCb due to the increase of gas flux from deep magma, which caused the increase of pressure and the thermal demagnetization. In addition, a large number of earthquakes occurred around the upper part of HCb which expanded the path of the ascending volcanic gases.
3. The pathway penetrating HCb emerged as a result of the repeated occurrence of earthquakes, thus allowing the ascent of larger fluxes of volcanic gases. The high-temperature gases reached the aquifer, which occupies an extensive region around the upper part of HCb (~300 m asl). The heat of volcanic gases was efficiently transported to the surrounding rocks through the groundwater, which caused the observed geomagnetic field variations indicating abrupt thermal demagnetization. The part of the volcanic gases which was mixed with groundwater was discharged from the fumaroles and the remaining gas was spread aside through the aquifer.
4. Rapid heating occurring as a result of the increase of the gas flux from the deep-seated magma, and the diffusion of heat through the groundwater was repeated. As a result, the high-temperature zone, which was determined as the demagnetized zone, was expanded, and inflation was repeated since HCa containing clay-rich materials located above the aquifer acts as a cap. The volcanic gases continued to ascend by expanding the pathway connected to the fumaroles, which was observed in the form of shallow earthquakes beneath the crater and intense fumarolic activity.

6. Conclusions

Changes in the total geomagnetic intensity have been detected at Kuchi-erabu-jima volcano since 2001. The variations are in good agreement with several characteristics of the inflated volcanic activity, such as high seismicity, ground deformation, and changes in the chemical composition of fumarolic gases. The volcanomagnetic variations are produced by demagnetization of rocks beneath the area around the Shin-dake crater, which is considered to be caused by the changes in the thermal state of the shallow subsurface. Modeling of the demagnetization sources revealed that the source was located about 200 m below sea level until 2002 and at about 300 m above sea level since 2003.

We conducted an audio-frequency magnetotelluric survey to reveal the shallow resistivity structure beneath the summit area and discovered two conductive layers which were interpreted as hydrothermally altered layers containing clay-rich minerals. Due to their low permeability, they act as caprock for the hydrothermal fluids from the deep magma and as bedrock for the infiltrating meteoric water. The estimated source of demagnetization until 2002 was located at the lower part of the deep conductor, where high-temperature volcanic gases were temporarily accumulated since the low-permeability layer blocked the ascent. It is considered that after 2003, a large flux of high-temperature gases was able to penetrate the low-permeability conductive layer and to reach the aquifer, which was most likely formed around the upper boundary of the conductor. In addition, it was assumed that the heat was efficiently transported to the surrounding rocks through the groundwater in that region, and as a result thermal demagnetization was observed.

The increase of the magmatic gas flux caused a repeated and extensive thermal demagnetization, as well as ground deformation. The thermal and mechanical energy accumulated beneath the shallow conductor. The accumulated energy was released by discharges of the volcanic gases through the fumaroles, thereby causing volcanic earthquakes of various kinds, and by diffusion through the aquifer, which occupies an extensive region within the edifice. Although the stable path of volcanic gases to the ground surface around the Shin-dake crater was already established, if an even larger flux of volcanic gases is supplied, phreatic explosion might occur beneath the shallow capping layer. This study strongly suggests that the hydrothermally altered low-permeability layers and the aquifer formed above these layers play an important role in accumulating and releasing the energy of phreatic explosions.

Acknowledgements

We would like to thank K. Ishihara and the staff at Sakurajima Volcano Research Center (DPRI, Kyoto Univ.) for their continuous support and constructive discussions. A number of discussions with J. Hirabayashi and K. Nogami (Tokyo Inst. Tech.) were extremely helpful for inferring the characteristics of the hydrothermal system within the volcano. Continuous geomagnetic field observation has been maintained with the invaluable help of M. Iguchi, T. Tameguri, M. Fukushima, S. Maryanto, K. Aizawa, T. Yamazaki (Kyoto Univ.), S. Sakanaka (Akita Univ.), and H. Hase (Hokkaido Univ.). Reference data used in the time series analysis of the geomagnetic field were obtained by Kakioka Magnetic Observatory of JMA and were provided through World Data Center for Geomagnetism, Kyoto. We also express our gratitude to Y. Ogawa (Tokyo Inst. Tech.) for kindly granting the authors access to an MTU-5A system during the AMT survey in 2004 and for providing his software for performing inversion. We are also indebted to S. Sakai, Y. Fujimoto (Kumamoto Univ.), Y. Okada, and S. Yamaguchi (Kyoto Univ.) for their support with regard to data acquisition, to D. Miki (Kyoto Univ.) for instructing the rock magnetic experiments, and to H. Triastuty (Kyoto Univ.) for providing the list of hypocenters. Our thanks also go to the two reviewers (A. W. Hurst and Y. Sasai) for their constructive comments and suggestions to improve the manuscript. Most figures were prepared using the Generic Mapping Tools (Wessel and Smith, 1991). This study was supported by a Grant-in-Aid of MEXT for Encouragement of Scientists (No. 12740261: W. Kanda) and a Grant-in-Aid for Scientific Research on Priority Areas (Dynamics of Volcanic Explosion, Area No.422: Y. Ida).

References

Akaike, H., 1973. Information theory and an extension of the maximum likelihood principle. In: Petrov, B.N., Csaki, F. (Eds.), 2nd International Symposium on Information Theory. Akademiai Kaido, Budapest, pp.267−281.

Aramaki, S., 1969. Notes of the geology of Kuchi-no-erabu volcano, southern Japan (in Japanese with English Abstracts). Bull. Volcanol. Soc. Jpn. 14, 127−132.

Bahr, K., 1991. Geological noise in magnetotelluric data: a classification of distortion types. Phys. Earth Planet. Inter. 66, 24−38.

Barberi, F., Bertagnini, A., Landi, P., Principe, C., 1992. A review on phreatic eruptions and their precursors. J. Volcanol. Geotherm. Res. 52, 231−246.

Clark, D.A., Saul, S.J., Emerson, D.W., 1986. Magnetic and gravity anomalies of a triaxial ellipsoid. Explor. Geophys. 17, 189−200.

Courteaud, M., Ritz, M., Robineau, B., Join, J.L., Coudray, J., 1997. New geological and hydrogeological implications of the resistivity distribution inferred from audiomagnetotellurics over La Fournaise young shield volcano (Reunion Island). J. Hydrol. 203, 93−100.

Del Negro, C., Currenti, G., Napoli, R., Vicari, A., 2004. Volcanomagnetic changes accompanying the onset of the 2002–2003 eruption of Mt. Etna (Italy). Earth Planet. Sci. Lett. 229, 1−14.

DPRI, Kyoto University, 1992. The activities of volcanic eruptions and earthquakes at volcanoes in Satsunan Island (January 1991 ~ May 1992) (in Japanese). Rep. Coordinating Committee for Prediction of Volcanic Eruption 53, 101−107.

DPRI, Kyoto University, Tokyo Institute of Technology, Kagoshima University, 1981. Eruption of Shin-dake, Kuchinoerabu-shima, on Sep. 28, 1980 (Preliminary Report) (in Japanese). Rep. Coordinating Committee for Prediction of Volcanic Eruption 20, 1−9.

Efron, B., Tibshirani, R.J., 1993. An introduction to the bootstrap. Chapman and Hall. 456 p.

Fujii, I., Kanda, W., 2008. New procedures to decompose geomagnetic field variations and application to volcanic activity. Geophys. J. Int. 175, 400−414.

Geshi, N., Kobayashi, T., 2006. Volcanic activities of Kuchinoerabujima volcano within the last 30,000 years (in Japanese with English abstracts). Bull. Volcanol. Soc. Jpn. 51, 1−20.

Geshi, N., Kobayashi, T., 2007. Geological map of Volcanoes 14; Geological map of Kuchinoerabujima volcano 1:25,000 (in Japanese). Geological Survey of Japan, AIST, Tsukuba.

Groom, R.W., Bailey, R.C., 1989. Decomposition of magnetotelluric impedance tensors in the presence of local three-dimensional galvanic distortion. J. Geophys. Res. 94, 1913−1925.

Hirabayashi, J., Nogami, K., Suzuki, T., Mizuhashi, M., 2002. Volcanic gases and hot springs in Kuchierabujima (in Japanese). In: Sakurajima Volcano Research Center (Ed.), Report on Joint Observations at Satsuma-Iwojima and Kuchinoerabujima Volcanoes 2000. DPRI, Kyoto University, pp.143−152.

Hirabayashi, J., Nogami, K., Ohshima, H., Iguchi, M., 2007. The relationship between the chemical composition of volcanic gas from Kuchinoerabujima and its volcanic activity (in Japanese with English abstracts). Ann. Disas. Prev. Res. Inst., Kyoto Univ. 50 B, 359−364.

Hurst, A.W., Rickerby, P.C., Scott, B.J., Hashimoto, T., 2004. Magnetic field changes on White Island, New Zealand, and the value of magnetic changes for eruption forecasting. J. Volcanol. Geotherm. Res. 136, 53−70.

Iguchi, M., Yamamoto, K., Takayama, T., Maekawa, T., Nishimura, T., Hashino, H., Yakiwara, H., Hirano, S., 2001. Characteristics of volcanic earthquakes at Kuchierabujima volcano − Geophysical and geochemical joint observation 2000 − (in Japanese with English abstracts). Ann. Disas. Prev. Res. Inst., Kyoto Univ. 44 B-1, 317−326.

Iguchi, M., Yamamoto, K., Miki, D., Takayama, T., Teraishi, M., Sonoda, Y., Fujiki, S., Onizawa, S., Suzuki, A., Yakiwara, H., Hirano, S., 2002. Recent ground deformation at Kuchierabujima volcano (in Japanese with English abstracts). Ann. Disas. Prev. Res. Inst., Kyoto Univ. 45 B, 601−608.

Iguchi, M., 2007. Detection of change of anomalous geothermal area by aerial infrared thermal measurements at Kuchinoerabujima volcano (in Japanese). In: Iguchi, M. (Ed.), Practical study on prediction of phreatic eruption and its change at Kuchinoerabujima Volcano, Japan. DPRI, Kyoto University, pp.45−50.

Iguchi, M., Saito, E., Tameguri, T., Triastuty, H., Yamazaki, T., 2007. Evaluation of volcanic activity of Kuchinoerabujima in 2006 (in Japanese with English abstracts). Ann. Disas. Prev. Res. Inst., Kyoto Univ. 50 B, 349−357.

Ishihara, K., 1990. Pressure sources and induced ground deformation associated with explosive eruptions at an andesitic volcano: Sakurajima volcano, Japan. In: Ryan, M.P. (Ed.), Magma transport and storage. John Wiley & Sons, Chichester, pp.335−356.

Johnston, M.J.S., Mueller, R.J., Dvorak, J., 1981. Volcanomagnetic observations during eruptions, May-August 1980. In: Lipman, P.W., Mullineaux, D.R. (Eds.), The 1980 eruptions of Mount St. Helens, Washington. Geol. Surv. Profess. Paper 1250, pp.183−189.

Kanda, W., Tanaka, Y., Utsugi, M., Iguchi, M., Ishihara, K., 2001. Monitoring geomagnetic total intensity using satellite telecommunication at Kuchierabujima volcano (in Japanese with English abstracts). Ann. Disas. Prev. Res. Inst., Kyoto Univ. 44 B-1, 327−332.

Kanda, W., Tanaka, Y., Utsugi, M., Takakura, S., Hashimoto, T., Inoue, H., 2008. A preparation zone for volcanic explosions beneath Naka-dake crater, Aso volcano, as inferred from magnetotelluric surveys. J. Volcanol. Geotherm. Res. 178, 32−45.

Lénat, J.-F., Fitterman, D., Jackson, D.B., Labazuy, P, 2000. Geoelectrical structure of the central zone of Piton de la Fournaise volcano (Reunion), Bull. Volcanol. 62, 75−89.

Lopez, D.L., Williams, S.N., 1993. Catastrophic volcanic collapse: Relation to hydrothermal processes, Science 260, 1794−1796.

Matsumoto, H., 1960. The chemical characteristics of the lavas from Ryukyu volcanic zone, Kyushu, Japan. Kumamoto J. Sci. Ser. B. Sec. 1, Geology 4, 13−29.

Matsumoto, T., Ueno, H., Kobayashi, T., 2007. A new secular variation curve for South Kyushu, Japan, and its application to the dating of some lava flows. Rep. Fac. Sci, Kagoshima Univ. 40, 35−49.

Miki, D., 1995. Magnetically shielded room and instruments for paleomagnetic measurements (in Japanese with English abstracts). Ann. Disas. Prev. Res. Inst., Kyoto Univ. 38 B-1, 1−11.

Miki, D., Iguchi, M., Eto, T., Solihin, A., 2002. Paleomagnetic estimate of the ages of lava flows from Shindake at Kuchierabujima volcano (in Japanese). In: Sakurajima Volcano Research Center (Ed.), Report on Joint Observations at Satsuma-Iwojima and Kuchinoerabujima Volcanoes 2000. DPRI, Kyoto University, pp.159−168.

Nakada, S., Simizu, H., Ohta, K., 1999. Overview of the 1990–1995 eruption at Unzen Volcano. J. Volcanol. Geotherm. Res. 89, 1−22.

Nurhasan, Ogawa, Y., Ujihara, N., Tank, S.B., Honkura, Y., Onizawa, S., Mori, T., Makino, M., 2006. Two electrical conductors beneath Kusatsu-Shirane volcano, Japan, imaged by audiomagnetotellurics, and their implications for the hydrothermal system. Earth Planets Space 58, 1053−1059.

Ogawa, Y., Uchida, T., 1996. A two-dimensional magnetotelluric inversion assuming Gaussian static shift. Geophys. J. Int. 126, 69−76.

Ohba, T., Hirabayashi, J., Yoshida, M., 1994. Equilibrium temperature and redox state of volcanic gas at Unzen volcano, Japan. J. Volcanol. Geotherm. Res. 60, 263−72.

Parkinson, W.D., 1962. The influence of continents and oceans on geomagnetic variations. Geophys. J. R. Astron. Soc. 6, 441−449.

Saito, E., Iguchi, M., 2006. Ground deformation detection at Kuchinoerabujima volcano by continuous GPS with simple atmospheric correction (in Japanese with English abstracts). Bull. Volcanol. Soc. Jpn. 51, 21−30.

Saito, E., Iguchi, M., 2007. GPS monitoring results at Kuchinoerabujima volcano − April 2004 to December 2006 − (in Japanese). In: Iguchi, M. (Ed.), Practical study on prediction of phreatic eruption and its change at Kuchinoerabujima Volcano, Japan. DPRI, Kyoto University, pp.21−24.

Sasai, Y., 1991. Tectonomagnetic modeling on the basis of the linear piezomagnetic effect. Bull. Earthq. Res. Inst., Univ. Tokyo 66, 585−722.

Sasai, Y., 2006. Magnetic field produced by a uniformly magnetized triaxial ellipsoid (in Japanese with English abstracts). Proc. 2006 Conductivity Anomaly Sympo., 151−157.

Tanaka, Y., 1993. Eruption mechanism as inferred from geomagnetic changes with special attention to the 1989−1990 activity of Aso volcano. J. Volcanol. Geotherm. Res. 56, 319−338.

Tanakadate, S., 1938. Eruptions of Shin-dake on Kuchi-no-erabu-jima: morphology of the crater and debris avalanches on Mukaehama (in Japanese). Kazan 3, 339−354.

Tomita, K., Kawano, M., Kobayashi, T., 1994. Minerals in the volcanic ash erupted from Shin-dake in Kuchinoerabu Island in 1980. Rep. Fac. Sci, Kagoshima Univ. 27, 1−10.

Triastuty, H., Iguchi, M., Tameguri, T., 2009. Temporal change of characteristics of shallow volcano-tectonic earthquakes associated with increase in volcanic activity at Kuchinoerabujima volcano, Japan (in press). J. Volcanol. Geotherm. Res. 187, 1−12, doi:10.1016/j.jvolgeores.2009.0517.

Utsugi, M., Tanaka, Y., Kanda, W., Matsushima, T., 2002. Aeromagnetic survey over Kuchierabujima volcano (in Japanese). In: Sakurajima Volcano Research Center (Ed.), Report on Joint Observations at Satsuma-Iwojima and Kuchinoerabujima Volcanoes 2000. DPRI, Kyoto University, pp.121−127.

Voight, B., Sparks, R.S.J., Miller, A.D., Stewart, R.C., Hoblitt, R.P., Clarke, A., Ewart, J., Aspinall, W.P., Baptie, B., Calder, E.S., Cole, P., Druitt, T.H., Hartford, C., Herd, R.A., Jackson, P., Lejeune, A.M., Lockhart, A.B., Loughlin, S.C., Luckett, R., Lynch, L., Norton, G.E., Robertson, R., Watson, I.M., Watts, R., Young, S.R., 1999. Magma Flow Instability and Cyclic Activity at Soufriere Hills Volcano, Montserrat, British West Indies. Science 283, 1138−1143.

Wessel, P., Smith, W. H. F., 1991. Free software helps map and display data. EOS Trans. AGU 72, 445−446.

Yamamoto, K., Iguchi, M., Takayama, T., Ishihara, K., 1997. Increase in seismic activity in 1996 at Kuchierabujima volcano (in Japanese with English abstracts). Ann. Disas. Prev. Res. Inst., Kyoto Univ., 40 B-1, 39−47.

Yukutake, T., Utada, H., Yoshino, T., Watanabe, H., Hamano, Y., Sasai, Y., Kimoto, E., Otani, K., Shimomura, T., 1990. Changes in the geomagnetic total intensity observed before the eruption of Oshima volcano in 1986. J. Geomag. Geoelec. 42, 277−290.

Zlotnicki, J., Bof, M., 1998. Volcanomagnetic signals associated with the quasi-static continuous activity of the andesitic Merapi volcano (Indonesia). Phys. Earth Planet. Inter. 105, 119−130.

Zlotnicki, J., Sasai, Y., Toutain, J. P., Villacorte, E. U., Bernard, A., Sabit, J. P., Gordon Jr., J. M., Corpuz, E. G., Harada, M., Punongbayan J. T., Hase, H., Nagao, T., 2009. Combined electromagnetic, geochemical and thermal surveys of Taal volcano (Philippines) during the period 2005-2006. Bull. Volcanol. 71, 29−47.

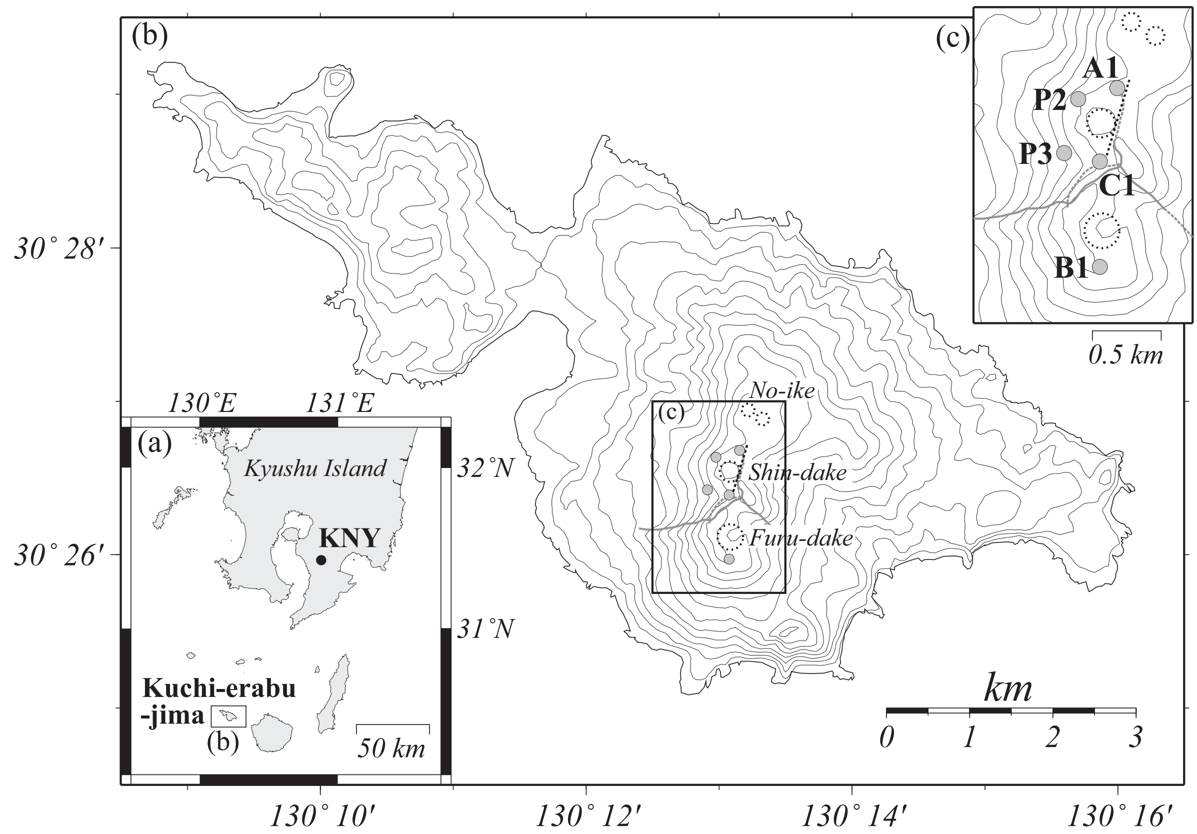

Figure 1: (a) Location of Kuchi-erabu-jima volcano and Kanoya Magnetic Observatory (KNY) of the Japan Meteorological Agency (JMA). (b) Topographic map of Kuchi-erabu-jima. Contour interval is 50 m. Major craters are denoted with dotted circles and lines. Gray solid (dashed) lines indicate (concealed) rims of slope failure of Furu-dake (Geshi and Kobayashi, 2006). (c) Detailed map of the summit area. Gray circles show the locations of magnetic stations.

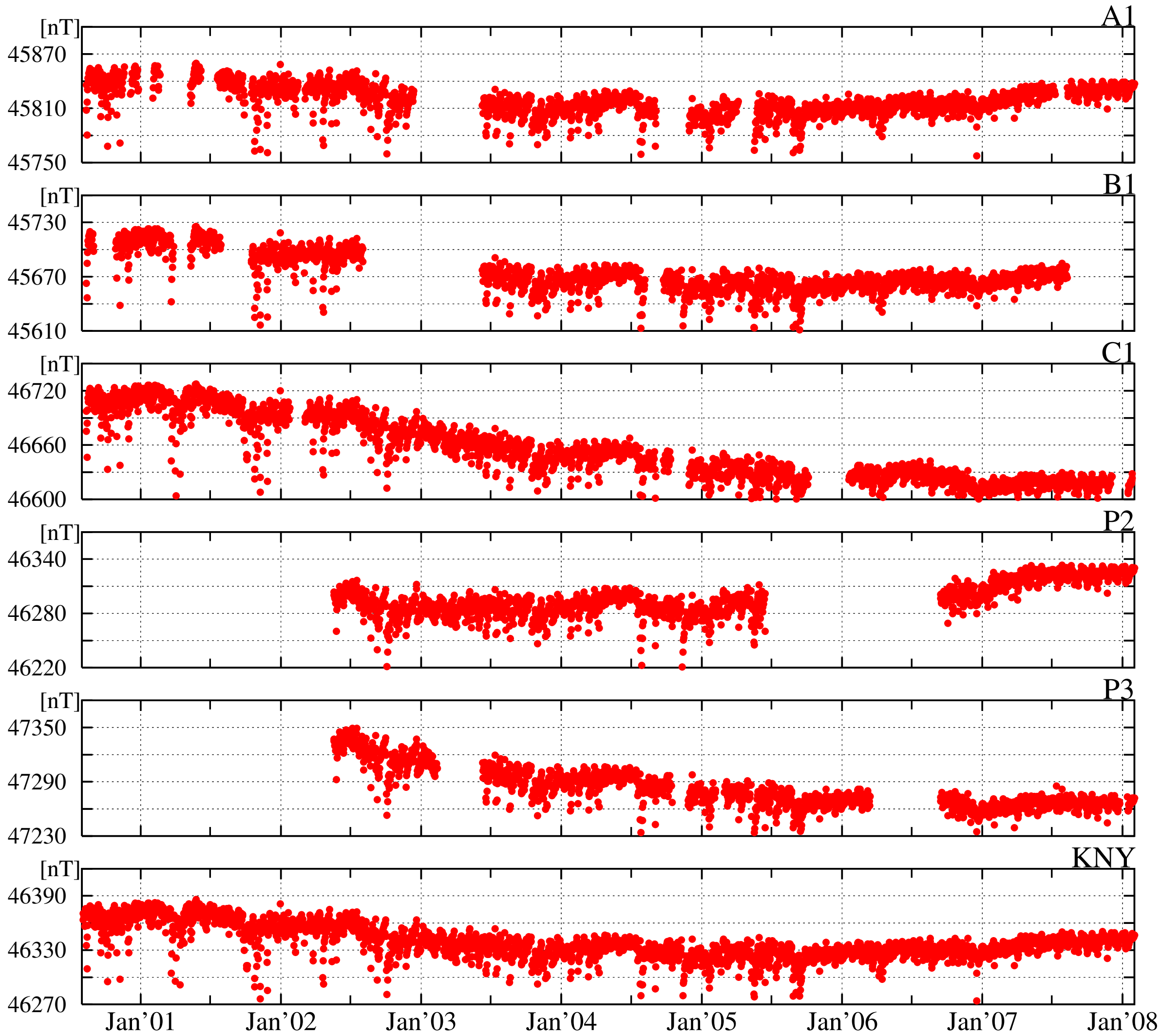

Figure 2: Total geomagnetic intensities observed at five sites at Kuchi-erabu-jima volcano and at KNY. Daily means are shown. Vertical scale for each panel is set to 150 nT with a grid interval of 30 nT.

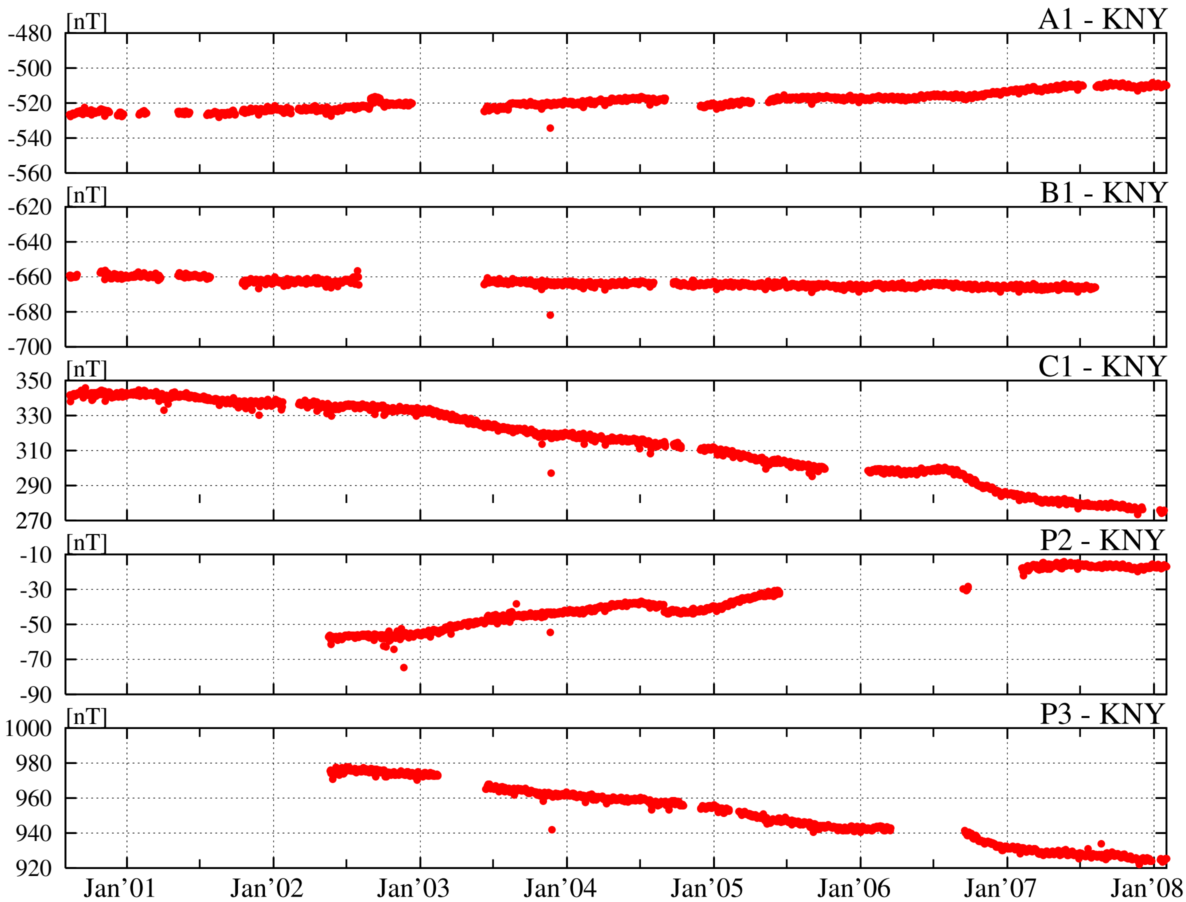

Figure 3: Simple differences of data observed at five stations with respect to those at KNY. Hourly averaged values were differenced and nighttime means (00:00 – 04:59 JST) are shown. Vertical scale for each panel is set to 80 nT with a grid interval of 20 nT.

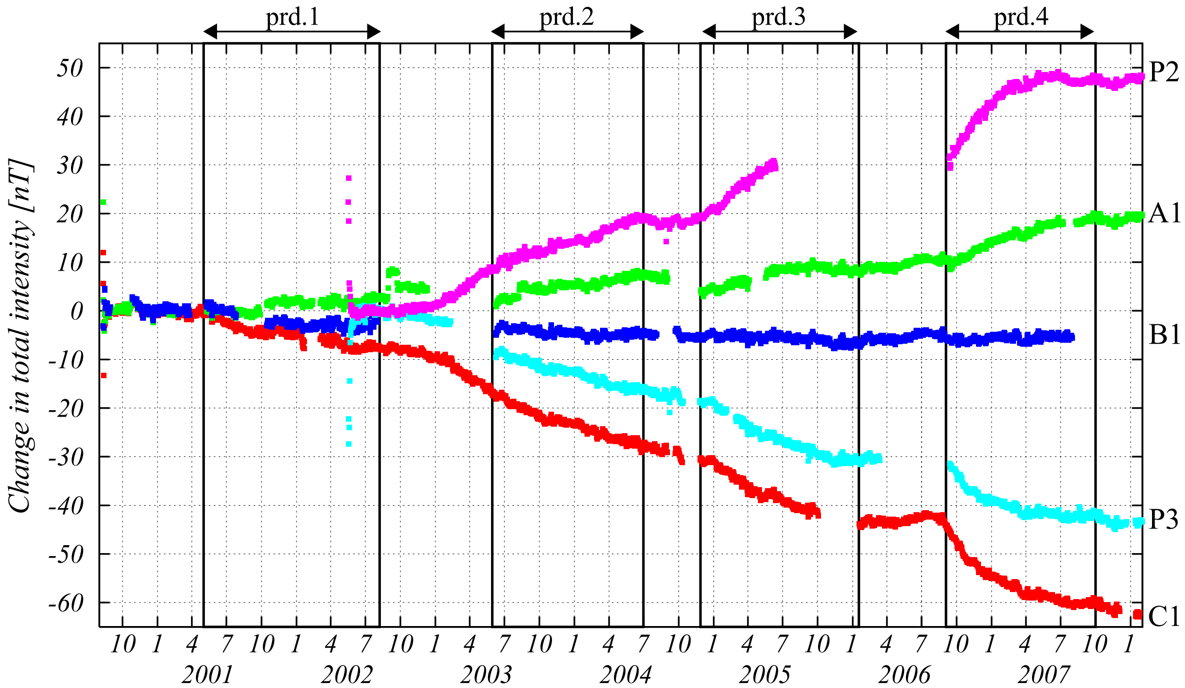

Figure 4: Trend components of five sites estimated from time series analysis. Zero level is adjusted to Aug. 10, 2000 for sites A1, B1, and C1 and to May 17, 2002 for the other two sites. Grid intervals are set to 3 months along the horizontal axis and to 10 nT along the vertical axis. Nighttime means are shown.

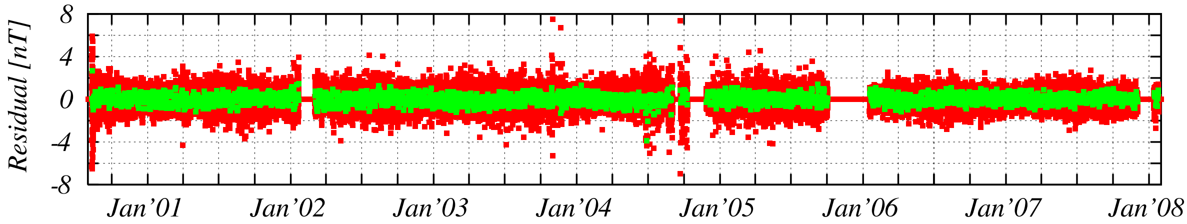

Figure 5: Residual between observed and estimated time series for site C1. Red dots indicate the residuals of hourly values used for the Kalman filter method. Green dots show those of nighttime means. Grid interval along the vertical axis is 2 nT.

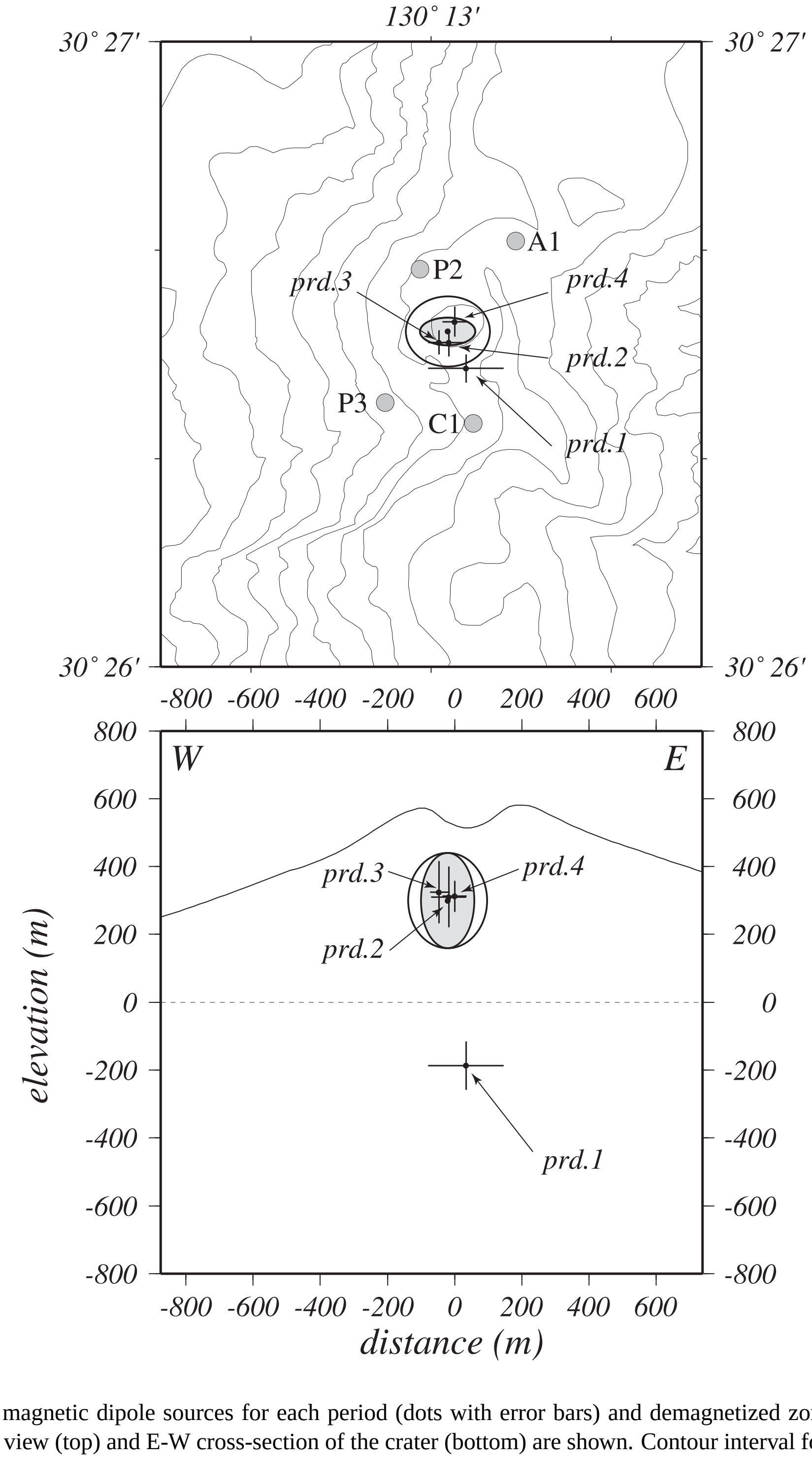

Figure 6: Estimated magnetic dipole sources for each period (dots with error bars) and demagnetized zones between prd.2 and prd.4 (ellipses). Plan view (top) and E-W cross-section of the crater (bottom) are shown. Contour interval for the topography is 50 m. Shaded ellipse indicates the projection of the demagnetized ellipsoid during prd.2, and open ellipse is the expanded zone at the end of prd.4.

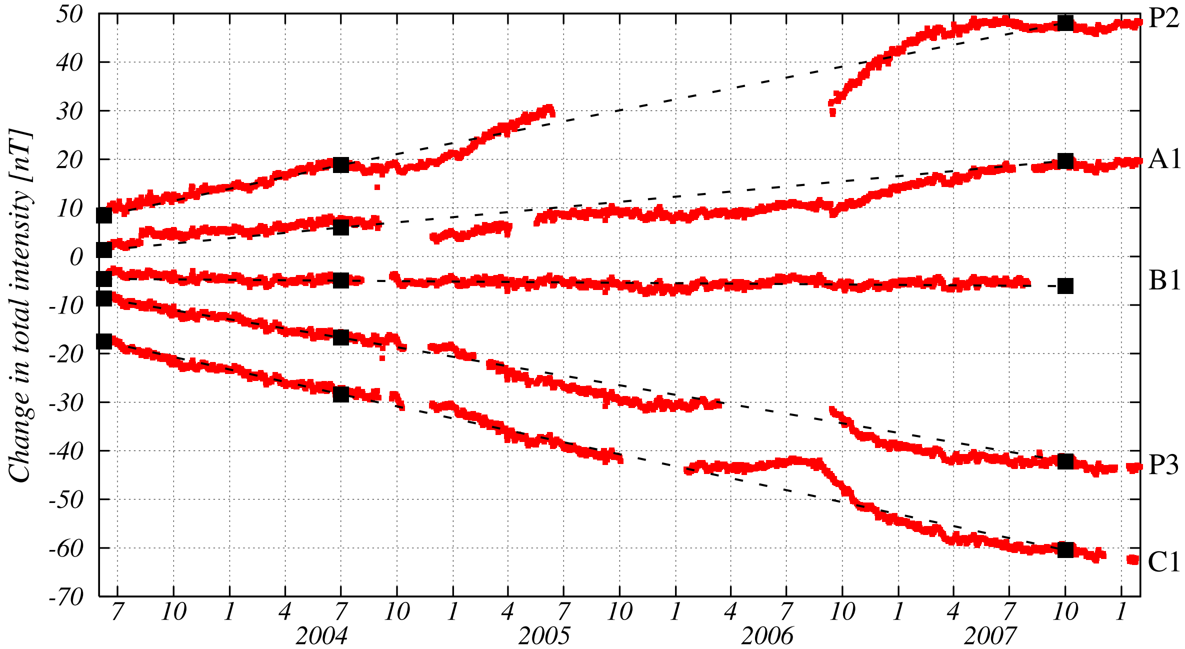

Figure 7: Comparison of total intensity changes at 5 sites. Changes expected at the end of prd.2 and prd.4 for models of the demagnetized ellipsoids (squares with dashed lines) shown in Fig. 6 and the estimated volcanomagnetic variations (Fig. 4: red) after prd.2 are shown. Calculated value at each site is offset by the first datum of prd.2 (June 9, 2003).

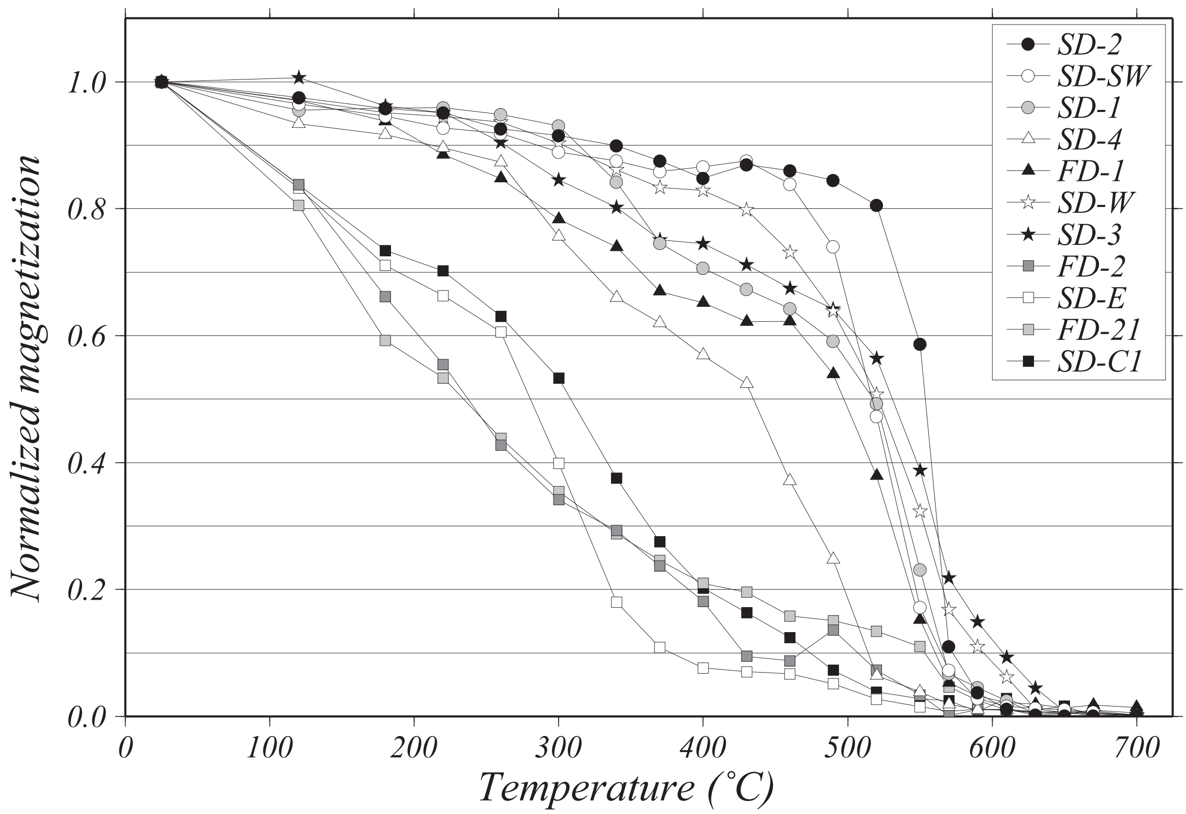

Figure 8: Thermal demagnetization curves for 11 samples. Magnetization intensity is normalized over the initial magnetization of each sample. Rock samples with similar features are denoted with the same symbols (see the text).

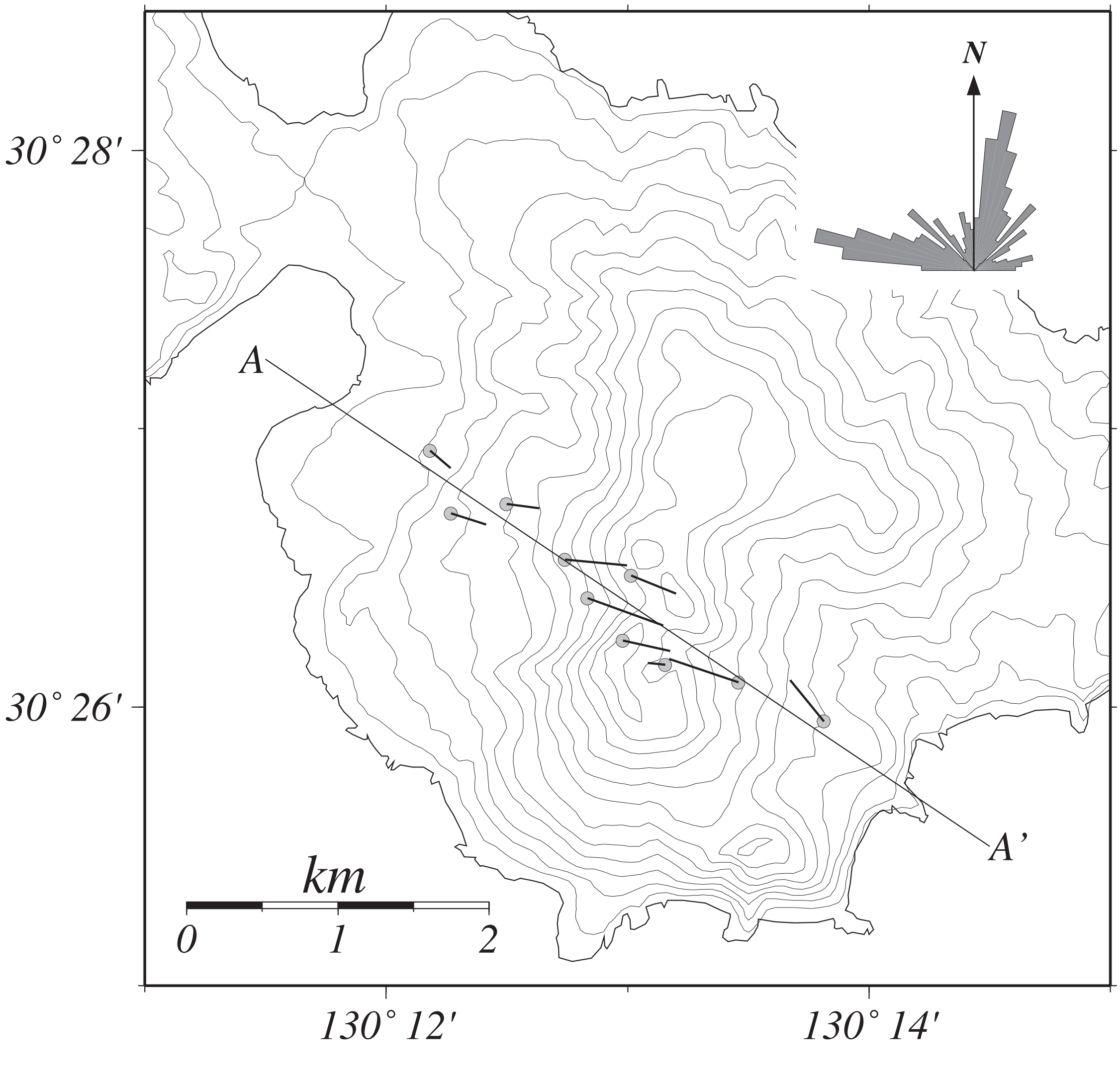

Figure 9: Site location of the AMT survey carried out in November 2004. A–A’ represents the profile of the 2-D inversion shown in Fig. 10. Arrows indicate the real part of the induction vectors (Parkinson’s convention) at 97 Hz. Inset shows polar histograms of the estimated strike for all frequencies as obtained with the tensor decomposition technique (Groom and Bailey, 1989). Sector width is 5 degrees and strike directions intrinsically have the ambiguity of 90 degrees.

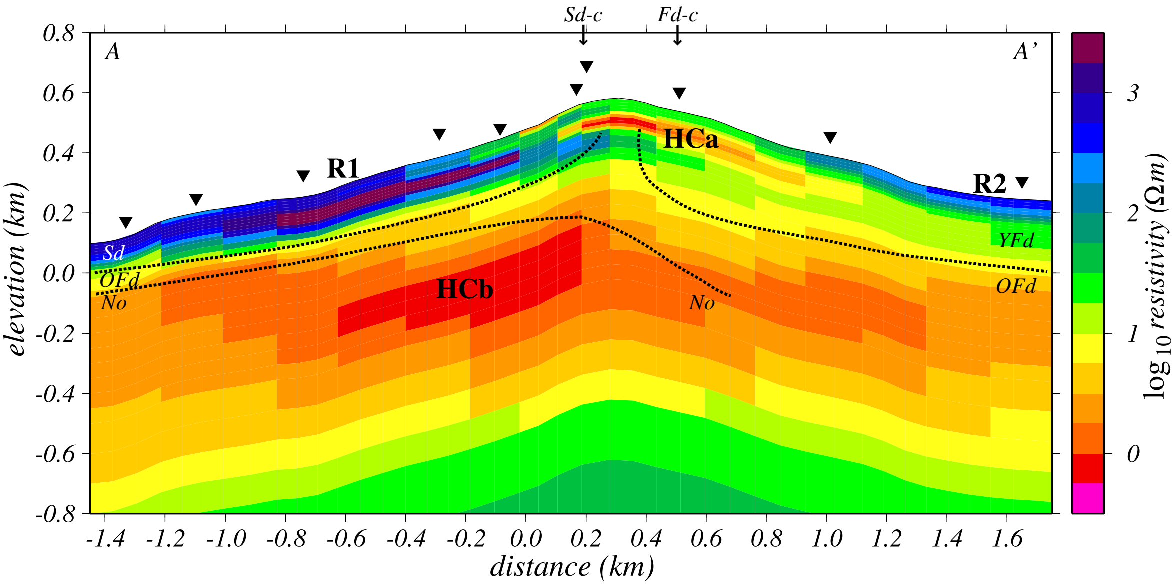

Figure 10: Final 2-D resistivity model inferred from the TM-mode data of the A–A' profile (Fig. 9). The profile is projected onto the section perpendicular to the assumed strike direction (N13°E). Inverse triangles indicate locations of the AMT sites. Major conductive regions are labeled as HCa and HCb, while resistive ones are labeled as R1 and R2. Dotted lines indicate the presumed boundaries of the volcanic edifices from geological studies (Geshi and Kobayashi, 2006, 2007). *Sd*: Shin-dake, *YFd*: Younger Furu-dake, *OFd*: Older Furu-dake, *No*: No-ike. *Sd-c* and *Fd-c* denote the craters of Shin-dake and Furu-dake, respectively. There is no vertical exaggeration in the graphs.

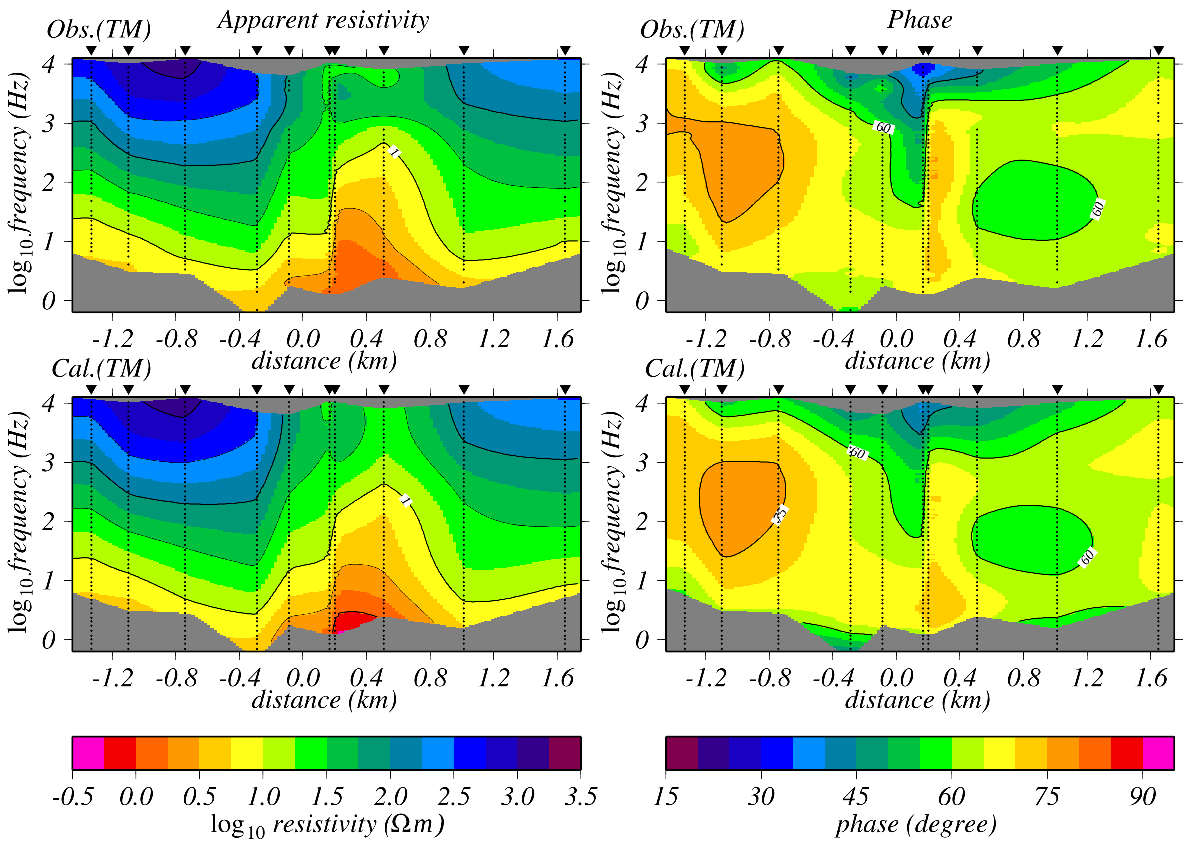

Figure 11: Pseudo-sections of observed data (top) and inverted model responses (bottom) for the A–A' profile shown in Fig. 9. Left and right rows show apparent resistivity and phase of the TM-mode, respectively. Black dots indicate the presence of data used in this study.

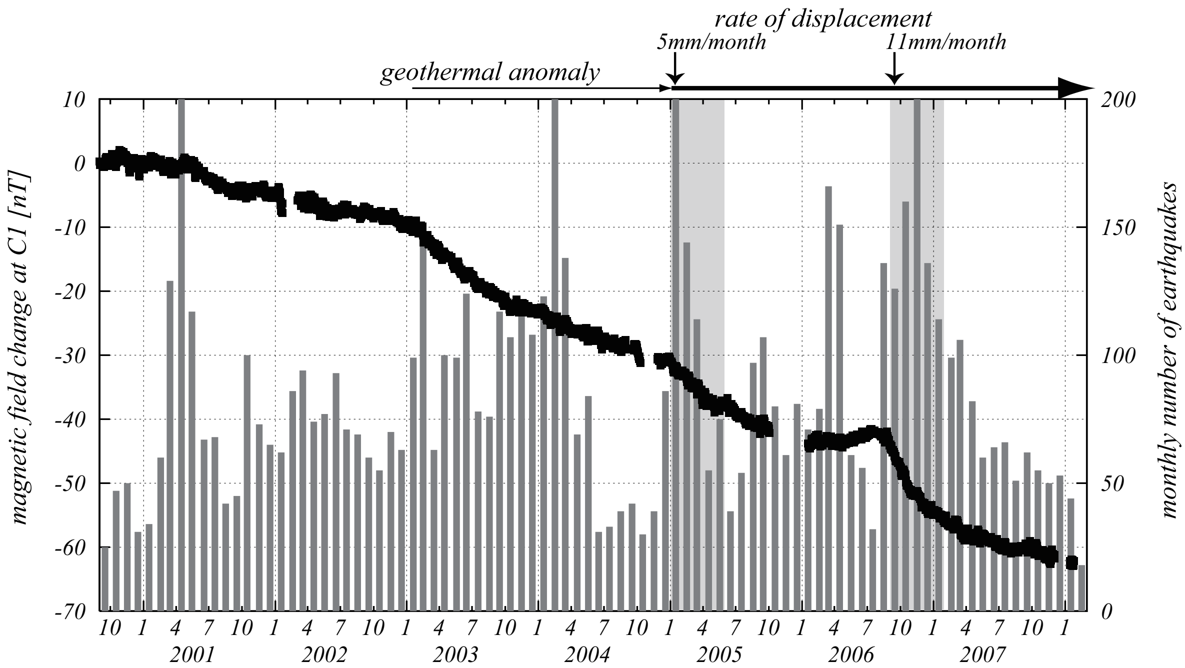

Figure 12: Estimated magnetic variation at site C1 (left axis) and monthly number of volcanic earthquakes (right axis) observed at a seismic station located on the western flank of Shin-dake. Shaded areas indicate periods of notable inflation as detected by the continuous GPS network, which was established in April 2004 (Saito and Iguchi, 2006). We also indicate the rates of horizontal displacement observed around the crater in the initial stage of each inflation period (Saito and Iguchi, 2007). We are not in possession of continuous GPS data for the elevated activity in 2003. Arrows indicate a period of anomalous geothermal activity around the Shin-dake crater, which was identified in February 2003 and became larger after January 2005.

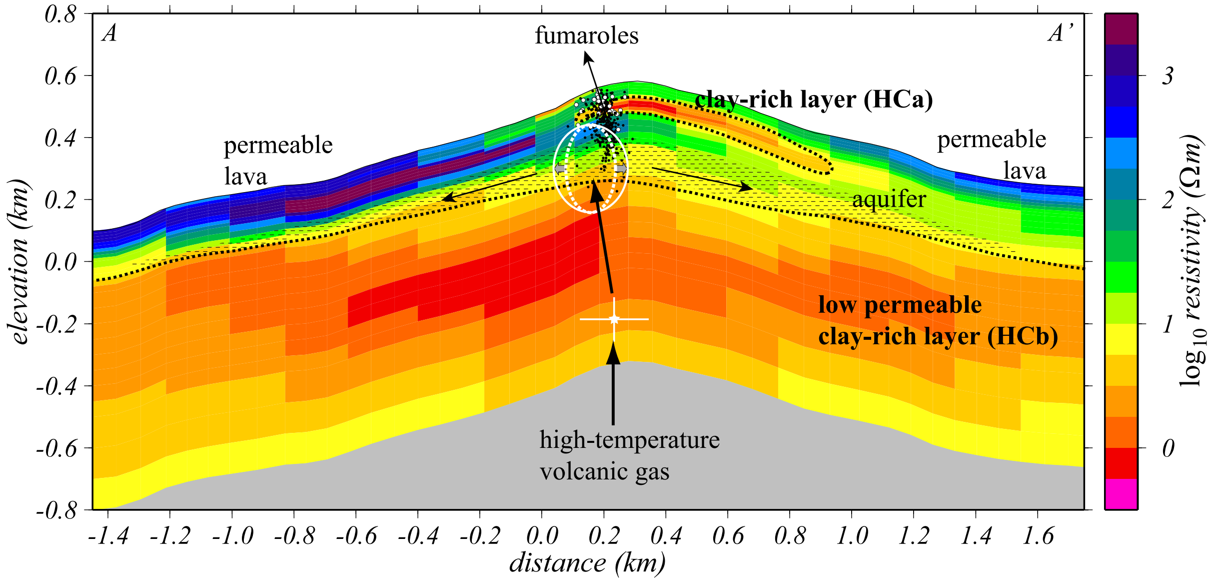

Figure 13: Conceptual model of the heating process inferred from this study. Black and white dots indicate hypocenters of HF and LF earthquakes observed in 2006 (Triastuty et al., 2009). Ellipses and a star with error bars represent demagnetized sources and indicate the projection of Fig. 6 to the resistivity section. Arrows indicate the path of high-temperature volcanic gases supplied from deep-seated magma. Hatched area located above the conductive layer (HCb) is regarded as the aquifer. Area of low resolution is masked with gray.

Table 1: Optimum parameters for estimated time series models. τ_t^2 is fixed to $1.00{\times}10^{-5}$.

site	τ_o^2	τ_s^2	K	L
A1	0.483	$3.16{\times}10^{-5}$	2	14
B1	0.597	$1.78{\times}10^{-4}$	2	14
C1	0.466	$1.78{\times}10^{-4}$	2	15
P2	0.652	$3.16{\times}10^{-6}$	2	6
P3	0.521	$3.16{\times}10^{-6}$	2	14

Table 2: Estimated location and moment of the magnetic dipole source for each period. Origin of the coordinate system is set at sea level beneath the center of the Shin-dake crater. X, Y, and Z denote coordinates in meters in northward, eastward, and downward directions, respectively. M indicates intensity of magnetic moment in units of Tm^3. The error of each parameter shows the standard deviation calculated with a bootstrap method.

period	X	Y	Z	M
prd.1	-110 ± 41.5	$+33.6 \pm 113$	$+187 \pm 71.9$	$-1.25^{17.5\pm1.2}$
prd.2	-33.6 ± 41.1	-17.5 ± 52.2	-311 ± 89.3	$-1.25^{7.7\pm1.9}$
prd.3	-33.4 ± 36.0	-46.0 ± 32.3	-325 ± 91.9	$-1.25^{7.8\pm1.7}$
prd.4	$+27.8 \pm 44.2$	-0.10 ± 36.4	-312 ± 46.1	$-1.25^{9.9\pm1.4}$

Table 3: Estimated parameters of uniformly magnetized ellipsoid, where a, b, and c denote the respective half-axis lengths in northward, eastward, and downward directions in units of meters. ΔJ indicates magnetization intensity change in units of A/m, and R is the residual calculated as $\sqrt{\sum (obs. - cal.)^2}$ where *obs*. and *cal*. denote observed and calculated amounts of magnetic variation at a given site, respectively. Center of the ellipsoid was estimated to be located at (0, -20, -300) throughout all periods (Fig. 6).

prd.	a	b	c	ΔJ	R
2	40	80	140	-1.8	1.37
2-4	100	120	140	-1.9	0.857

Table 4: Natural remanent magnetization (NRM) and induced magnetization for 11 samples. n: number of specimens per rock sample. J_r: NRM in units of A/m. err: relative error of J_r in percent. χ: volume susceptibility in 10^{-3} SI units. J_i: induced magnetization in units of A/m, assuming ambient magnetic field intensity of 46,000 nT. Q: Koenigsberger ratio (J_r/J_i). J_t: total magnetization in units of A/m. Rock type of all samples is andesite.

sample	n	J_r	err	χ	J_i	Q	J_t
SD-2	7	17.89	0.38	41.3	1.51	11.8	19.4
SD-SW	4	6.44	0.79	1.52	0.56	11.5	6.99
SD-1	3	5.20	1.16	32.7	1.20	4.34	6.40
SD-4	6	1.45	0.90	34.4	1.26	1.15	2.71
FD-1	5	0.53	2.02	3.57	0.13	4.04	0.66
SD-W	4	1.93	1.14	2.14	0.78	2.46	2.72
SD-3	6	1.77	1.05	5.38	0.20	9.00	1.97
FD-2	4	1.27	1.36	27.5	1.01	1.26	2.27
SD-E	4	0.95	1.49	3.68	1.35	0.70	2.30
FD-21	4	0.74	1.39	19.2	0.70	1.04	1.44
SD-C1	6	0.61	1.19	43.6	1.60	0.38	2.20